ICSI 2019 The 3rd International Conference on Structural Integrity

Acquiring *in situ* Fatigue Crack Growth Curves by a Compliance Method for Micro Bending Beams to Reveal the Interaction of Fatigue Cracks with Grain Boundaries

Patrick Gruenewald[a], Jonas Rauber[a], Michael Marx[a], Christian Motz[a], Florian Schaefer[a,*]

[a]Dep. Materials Science and Methods, Saarland University, Campus D2 3, 66123 Saarbruecken, Germany

Abstract

To understand the interaction of dislocations with microstructural obstacles it is necessary to find test methods which are able to resolve the interaction of only a single or few defects with obstacles like interfaces. Therefore, the investigation of micro specimens has been established over the years as a suitable method to test the influence of microstructural features on the mechanical response. While quasi-static loading of micro specimens has been carried out extensively in the past decade and has given powerful insights on the mechanical behavior at small scales, cyclic loading and fatigue crack growth experiments still provide a challenge. In order to check the possibility to systematically initiate and monitor fatigue crack growth rates in micro specimens, we cyclically loaded micro bending beams made of a nickelbase superalloy. Furthermore, for grain boundaries of differing types we checked if the crack growth curves are suitable to measure crack - microstructure interactions. The fatigue cracks showed a deceleration when approaching the grain boundaries followed by an abrupt re-acceleration, which is in accordance to macroscopic experiments and connected to dislocation or slip transfer from the plastic zone of the crack through the grain boundary. Furthermore, we observed a dependency of the deceleration on the grain boundary type and the crystallographic orientation of the neighboring grains. A 3D-HR-orientation gradient map was gathered by HR-EBSD using the software CrossCourt in combination with a self-provided MATLAB tool to reveal detailed information about strain localization at the grain boundary in the process zone near the crack tip.

* Florian Schaefer. Tel.: +49-681-302-5172; fax: +49-681-302-5015.
  E-mail address: f.schaefer@matsci.uni-sb.de

Nomenclature

a	crack length
$\boldsymbol{\alpha}$	Nye's tensor
$\boldsymbol{b}$	Burgers vector
E	Young's modulus
$\boldsymbol{F}$	deformation gradient tensor
K	stress intensity factor
$\boldsymbol{\kappa}$	curvature tensor
J	J-integral
N	number of load cycles
R	stress ratio
ρ	density of geometrically necessary dislocations
$\boldsymbol{\sigma}$	stress tensor
θ	orientation vector
$\boldsymbol{\omega}$	rotation tensor
m,C	coefficients of fit

1. Introduction

Interfaces dominate the initiation and damage evolution in many materials. The interaction of cracks and the plastic zone with internal interfaces such as grain boundaries is one of the main mechanisms for an increase in lifetime of components if the interaction leads to a deceleration of the crack propagation during fatigue. However, this effect can be ambivalent as grain boundaries are also known to be main crack initiation sites during the fatigue of metals (Lang et al. (2017)). A detailed study of the interaction of fatigue cracks with grain boundaries is necessary to understand the mechanisms that determine whether grain boundaries act as factors that increase or as factors that decrease lifetime depending on their geometry (Knorr et al. 2015), constitution or deformation localization in their vicinity (Zhang et al. (1999)).

Understanding the interaction of cracks and grain boundaries requires a detailed knowledge of the interplay between the cracks themselves, the cracks' plastic zone and the grain boundaries. One experimental strategy is to acquire data from macroscopic fatigue tests by zooming in the process zone by high-resolution microscopy or high-resolution analysis methods like electron microscopy or focused ion beam tomography (FIB) (Kacher and Robertson (2012), Schaef et al. (2010)). Another way to gain insight is to downsize the experiment to exclude confounding factors for the evaluation and measurements and to achieve information that is inaccessible for tests on the macro scale such as the local grain boundary morphology or incompatibility stresses at grain boundaries in a polycrystalline compound of elastic anisotropic grains (Klusemann et al. 2013, Tiba et al. (2015)).

The aim of this investigation is to study how extremely small fatigue cracks with lengths of less than 10 µm interact with grain boundaries under bending deformation to get a high-resolution view of the dislocation - grain boundary interaction in the plastic zone. Therefore crack growth curves are gathered *in situ* using bicrystalline micro bending beams of a polycrystalline modification of the nickel base superalloy CMSX-4, prepared by FIB milling, in the scanning electron microscope (SEM). The interaction of the crack with the grain boundary leaves a typical fingerprint of a deceleration followed by a re-acceleration as known from macro fatigue tests with microstructural short fatigue cracks (Brueck et al. (2018), Krupp et al. (2010)). These micro crack growth curves provide detailed information on fatigue crack growth in the regime of the intrinsic fatigue crack propagation threshold proposed by Zerbst et al. (2016) and a new testing method for the quantification of the crack grain boundary interaction (Schaefer et al. 2017).

2. Experimental setup

2.1. Material selection

A stage-I fatigue crack growth of several hundred micrometers is characteristic for the face-centered cubic nickel-based superalloy CMSX-4. This crack growth behavior is promoted by a highly planar slip due to a precipitation hardening by coherent intermetallic precipitates. These long stage-I-cracks provide dislocation arrays on a single slip plane that has already been used to study the interaction of cracks with a couple of microstructural obstacles (Holzapfel et al. (2007), Schaef et al. (2011), Schaefer et al. (2016)). The method to initiate and monitor fatigue cracks in micro bending beams with a beam thickness of less than 15 µm was invented by Eisenhut et al. (2017) and enhanced for stage-II cracks growth by Gruenewald et al. (2018).

2.2. Specimen preparation

Bicrystalline micro bending beams were prepared containing selected grain boundaries with a chosen crystallographic misorientation $\Delta\theta$ and a chosen expected incompatibility stress state in a three-step process. The first step was to select the grain boundary after an orientation measurement by electron backscatter diffraction (EBSD) with Oxford Aztec in a Zeiss Sigma VP SEM. In a second step, the region for the FIB milling was cut free by cross-sectioning using Ar ion polishing. The subsequent FIB preparation was done with a FEI Helios Nanolab 600 at 30 kV acceleration voltage and an ion beam current of 21 nA and 6.5 nA Ga for the raw cuts. The final polishing was done at 0.92 nA and 0.48 nA in order to reduce Ga contamination of the surface of the bending specimens and to get the final dimensions of the beams, which were 15 µm x 15 µm in cross-section and a cantilever arm of 60 µm. A FIB-notch was cut on one side of the beams to get a first strong stress concentration for crack initiation. The notch was milled at 0.48 nA and sharpened at 28 pA. A more detailed description can be found in Eisenhut et al. (2017) and Gruenewald et al. (2018).

2.3. Loading procedure

The fatigue experiments were performed using an UNAT 2 *in situ* nanoindentation device from ASMEC/Zwick Roell in a Zeiss Sigma VP and a Tescan Vega XMH SEM. A gripper and a wedge were cut at the top of tungsten-carbide tips and used to drive the beams. For the crack initiation, the cyclic loading was carried out with the gripper in displacement control and drift was corrected manually. The displacement ratio R was set to -0.8 in order to achieve fast crack initiation at the notch and avoid a crack initiation on the notch-free side of the beams. After the cracks initiated, the beams were loaded in force control to get a more stable force level for the crack growth curve evaluation. Due to instrumental restrictions, a wedge and a stress ratio of 0.1 had to be used instead of the gripper. After switching to force control, the load was lowered below the displacement control level and only increased slowly to ensure that the fatigue cracks grow with a low ΔK. This approach is required since growing fatigue cracks, and the accompanying reduction in ligament in front of the crack, can lead to critical plastic deformation when the force is kept constant. For the same reason the force level had to be adjusted manually as soon as the fatigue cracks continued growing. The loading procedure, as well as the advantages and disadvantages of each loading phase, are summarized in Table 1.

Table 1. Parameters of the two phases of the loading procedure.

interval	control mode	R	advantage	disadvantage
initiation	displacement	-0.8	high stress concentration at notch tip for crack initiation	unstable load level, drift correction by hand
growth	force	0.1	stable load level to decrease scatter in crack growth curves	at constant applied load a growing crack results in increased stress in the beams, requirement to adjust load level by hand every few hundred cycles

2.4. Crack growth curves and relative deceleration

The crack growth rates da/dN were calculated by a combination of experimental data (force and displacement) and finite element method (FEM) co-simulations (geometry factor and crack length dependency of the stiffness). The crack length measured by the compliance method is more accurate on the micro scale compared to SEM micrographs because it provides a higher resolution. The stiffness of the beams was calculated for each loading cycle N from the measured force and displacement data. For each of the investigated beams, the stiffness of a micro bending beam with identical geometry and crystallographic orientation was calculated from the FEM simulations for different crack lengths a. Afterwards, the crack length was calculated from the comparison of measured and simulated stiffness values. As shown by Eisenhut (2017), the crack lengths calculated by this method are in a very good agreement to the crack lengths measured from SEM micrographs. A moving second order polynomial was then fitted to each data point and its neighboring data points. This polynomial was differentiated in regards of N to get the crack growth rate for each cycle da/d$N(a,N)$.

The geometry factor evolution was calculated by simulating the J-integral for different crack lengths and normalizing it in regards of the force squared. A sixth order polynomial was fitted to these force normalized $J(a)$ simulated data to get a geometry factor that can be used for further calculations of J for a measured force and crack length. With the measured force range and the calculated crack length the elastic ΔJ was calculated for each load cycle. Afterwards, the cyclic stress intensity factor ΔK was derived from ΔJ by using the elastic stiffness tensor in Voigt's notation and local crystallographic orientation of the beams.

The crack growth curves were constructed with the crack growth rate da/dN and the cyclic stress intensity factor ΔK for each beam. Similar to a Paris-Erdogan power law fit for long fatigue crack growth, a power law fit to the linear region of these crack growth curves was applied (Equation 1). The relative deceleration of the fatigue cracks when approaching the grain boundaries was calculated from the measured crack growth rate at the slowest point compared to the crack growth rate the crack would have according to the power law fit.

$$\frac{\mathrm{d}a}{\mathrm{d}N} = C\Delta K^{\mathrm{m}_{short}} \tag{1}$$

2.5. 3D-EBSD

Local lattice rotations are well-known to stand in close relationship with the crystal's plastic deformation. The former are readily available using EBSD. When dealing with plasticity, the most frequently used representation of rotation data is the kernel average misorientation (KAM), which is a useful, qualitative tool for distinguishing regions of high or low plastic deformation. A quantity less commonly used, yet containing more information, is Nye's tensor $\boldsymbol{\alpha}$, which can also be derived from EBSD data as shown by Pantleon (2008). This relationship is given in Equation 2 with $\boldsymbol{\theta}$ being the crystal orientation vector and $\boldsymbol{\kappa}$ the orientation gradient or lattice curvature.

$$\boldsymbol{\alpha} = \mathrm{rot}(\boldsymbol{\kappa}) = \begin{pmatrix} -\kappa_{22} - \kappa_{33} & \kappa_{21} & \kappa_{31} \\ \kappa_{12} & -\kappa_{11} - 33 & \kappa_{32} \\ \kappa_{13} & \kappa_{23} & -\kappa_{11} - \kappa_{22} \end{pmatrix} \tag{2}$$

Thus, Nye's tensor is a quantity describing a change of orientation, a curvature. It is directly linked to the density ρ of geometrically necessary dislocations (GNDs) in a given reference volume determined by the spacing of data points (EBSD step size), as each dislocation type also forces a characteristic curvature to the lattice. This relationship is given in Equation 3 which also provides an equation system to derive the density of each dislocation type $\boldsymbol{t}$ with Burgers vector $\boldsymbol{b}$ and dislocation line vector $\boldsymbol{l}$.

$$\alpha_{\mathrm{ij}} = \sum_{\mathrm{t}}^{\mathrm{T}} \rho^{\mathrm{t}} b_{\mathrm{i}}^{\mathrm{t}} l_{\mathrm{j}}^{\mathrm{t}} \tag{3}$$

However, to be able to detect all present GNDs in the reference volume, all nine components of the Nye tensor must be known which in turn requires the rotation gradient to be known in each direction, also in the depth direction. Thus, the sample must be cross-sectioned in order to create the complete Nye's tensor field. Also, EBSD data usually show orientation noise of about 0.5° resulting in a background in the GND density calculated using this method. A

somewhat novel method offering a higher angular precision is high resolution EBSD (HR-EBSD). It is a post processing technique where the recorded patterns of two data points A and B are compared to each other via digital image correlation (DIC) to determine the deformation gradient F describing the transformation of the lattice at point A to that of point B as developed by Wilkinson et al. (2006). From F the rotation tensor ω and thus the orientation gradient κ can be calculated with a higher precision compared to conventional EBSD. Therefore, a combination of EBSD tomography by FIB and HR-EBSD is promising to gain deeper insight into the bulk dislocation distribution in deformed volumes. In this work such a combined approach was used to analyze the fatigue induced dislocation density in a micro bending beam. However, as the commercial HR-EBSD software CrossCourt (Wilkinson et al. (2009)) only features the analysis of 2D EBSD data, some workarounds must be employed for a 3D analysis. Indeed, one must keep in mind that we only measure a density of GNDs, depending on the EBSD step size. However, the total dislocation density consists of GNDs and statistically stored dislocations (SSDs).

3. Grain boundary interaction

3.1. Crack growth curves

Using the methodology described in Section 2.4 we can evaluate the crack growth rate for each of the 5 fatigue cracks tested. Exemplary curves for grain boundary configurations with high and low crack resistance as represented by the relative deceleration of crack growth prior dislocation and crack transfer are shown in Fig. 1 (a) and (b). Even for the configuration where the deceleration effect is low the point where multiple data points deviate from the foregoing linear behavior can be determined. The increased slope in the rapid growth phase is also clearly observable. Yet, due to this rapid crack growth the micro specimens underwent a plastic collapse before the applied force could be adjusted accordingly, resulting in failure of the specimens and a low number of data points in this rapid growth regime (Fig. 1(c)).

An advantage of this method is the simultaneous observation of the crack during loading, which is essential to correlate the behavior of the crack growth curves to the position and path of the fatigue cracks at the exact same cycles. This correlation is demonstrated in Fig. 1(c) where the micrograph of one fatigue crack at the moment of maximum deceleration is shown. It can be clearly stated that the crack tip is right in front of the grain boundary without trespassing it, further underlining the fact that the measured deceleration is indeed due to interaction of the dislocations in the plastic zone of the crack with the grain boundary.

A summary of all measured crack growth curves is given in Table 2, including the power law fit parameters for each curve as well as the characteristics of each grain boundary configuration and the measured relative deceleration. The parameters of the linear fit, especially m_{short}, can be divided into two parts. For the configurations with small difference in Young's modulus, primarily aligned in <100> direction, we measured a value of around 9 and for the configurations with a high difference in the Young's modulus, primarily aligned in <110> direction, we measured a value of around 12. Yet, care has to be taken whether this deviation is truly correlated to the expected higher
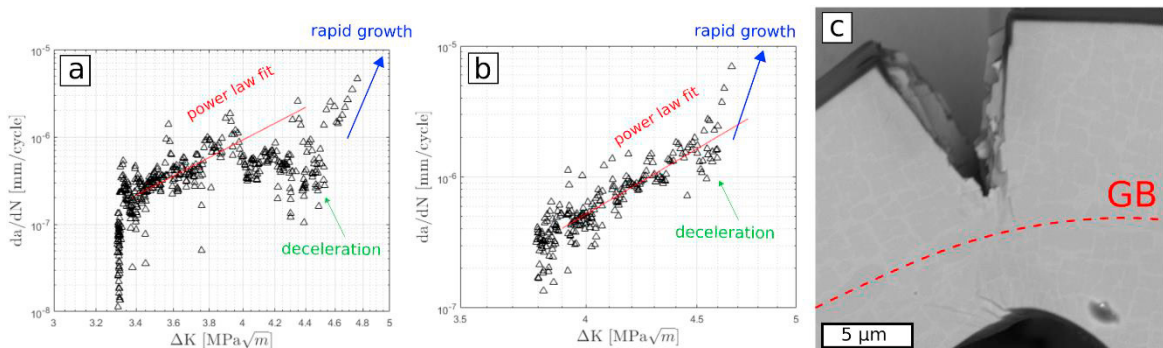
Fig. 1. Crack growth rate for a grain boundary setup with high (a) and low (b) deceleration. The linear phase where to data was fit to a Paris-Erdogan like power law, the point of deceleration and the rapid growth phase are marked in red, green and blue respectively. (c) SEM micrograph in backscattered electron (BSE) contrast of a fatigue crack approaching the grain boundary. The surface path of the grain boundary (GB) is marked with a dashed red line.

incompatibility stresses due to the elastic anisotropy in the <110> aligned case instead of the <100> aligned case or to one of the other parameters changing between the two types of configuration, namely the crystallographic orientation in direction of the loading axis or the number of active slip systems. The differences in *C* are not as pronounced, but it can be stated in general that the values for C for the high anisotropy configurations are lower than those for low anisotropy. Since these values correlate to the crack growth behavior before interacting with a grain boundary, the misorientation angle has no noticeable influence on these parameters.

3.2. Grain boundary resistance

The measured relative deceleration in Table 2 shows that each of the grain boundaries had a decelerating effect on the crack growth rate. The first grain boundary, which has been tested twice to check for the reproducibility (specimens 1 and 2), resulted in values for the relative deceleration which are close to each other with a difference of only around 10 %. Some of the other configurations, e.g. specimen 4 which corresponds to the curve in Fig. 1 (b), show less deceleration. Differences between both grain boundary configurations were therefore measurable.

The measurements of the relative deceleration show that both the high and small angle grain boundaries have one orientation to the beam axis with a high deceleration and one orientation to the beam axis with a lower deceleration. On average, the deceleration for the high angle grain boundary is higher than for the small angle grain boundary, indicating a higher resistance against slip transfer for the high angle grain boundary.

Furthermore, there is a strong difference between the orientations to the beam axis. We expected high elastic anisotropy stresses for the two beam axis orientations with a high difference in the Young's modulus between both adjacent grains and a low influence of elastic incompatibility for the case of a low difference in the Young's modulus. Yet, the difference in the deceleration at the grain boundary is opposed for the high and small angle grain boundaries. Whereas the small angle grain boundary shows a smaller resistance for the low anisotropy configuration (<100> crystal direction as beam axis), the higher resistance values are measured for the high anisotropy configuration of the high angle grain boundary (<110>).

The parameters describing the grain boundary configuration which are accessible beforehand do not fully describe the slip transfer resistance. Other missing factors are the number of active slip systems on each side of the grain boundary (see section 3.3), geometrical configurations of these slip systems and strength of the dislocation pileup at the grain boundary. Some of this information is available from the three dimensional EBSD evaluation. While previous experiments, where the grain boundary resistance was measured at the macroscale, were specifically tuned so that only a single slip system is active in the initial grain, the 3D-EBSD (Fig.2) results here, depict a complex deformation state along the crack path and in front of the crack tip. This complicates a geometrical evaluation of the slip resistance, as the number of potential slip system (12 potential slip systems for f.c.c in the outgoing grain) leads to a number of slip system couplings that is 12 times the number of active slip systems in the initial grain.

Table 2. Overview of the parameters describing the grain boundary configuration (ΔE, $\Delta \theta$) and the values needed to calculate the relative deceleration (m_{short}, C, ΔK_{start})

micro specimen	1	2	3	4	5
misorientation angle $\Delta \theta$ (°)		29.7			9.0	
ΔE, along the beam axis (GPa)		1.13	78.27	2.26	16.26
m_{short}	9.01	9.56	12.76	9.76	12.65
C	3.48E-12	5.34E-13	3.61E-14	6.95E-14	3.98E-15
ΔK_{start} (MPam$^{0.5}$)	3.32	3.46	3.23	3.61	3.94
relative deceleration (%)	82.23	92.05	65.22	31.54	81.42

3.3. Method and reproducibility

As all experiments on micro specimens are susceptible to large scatter in the measured data due to the large amount of influencing factors, the first question to arise is whether this method provides sufficient reproducibility. Due to the
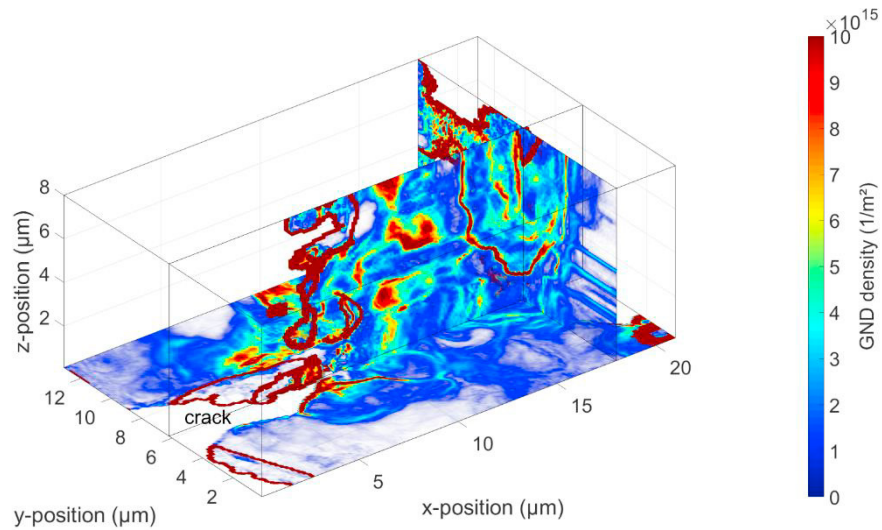
Fig. 2. GND density distribution in three selected slices of the tomographed beam volume, derived via deconvolution of Nye's tensor using a least squares fit to determine the dislocation configuration of lowest total density (highly underdefined equation system).

high experimental effort, it would have been infeasible to test a large amount of specimens for each grain boundary type and orientation. To test the reproducibility, we tested one of the configurations twice (specimens 1 and 2). Not only the two measured decelerations are in good agreement with each other, the slope of the da/dN curves prior grain boundary contact is in good agreement, too.

Besides the reproducibility of the grain boundary interaction we can also consider the crack growth curves themselves. It can be shown that for similar crystallographic orientations (specimens 1/2/4 and specimens 3/5) the slopes of the power law fit are comparable to each other, indicating that for the same orientation the determination of the crack growth rate is consistent and that there is a measurable difference between different crystallographic orientations. In the <100> loading direction with lower m_{short} of about 9 there are two approximately equivalent slip directions on all 4 slip planes that have a similar Schmid factor of ~0.408. For the <110> case only two slip planes are active and each has two slip directions with a Schmid factor of ~0.408. Therefore, we derive, that for the case of a higher number of 8 active slip directions in the <100> case compared to only 4 active ones in the <110> case, the coefficient m_{short} is lower and therefore crack growth is slower. A higher dislocation immobility due to dislocation interactions might be the reason for this in the <100> case.

3.4. 3D-EBSD

Orientation noise and spikes usually present in EBSD data were reduced using a component-wise quaternion median filter. As depicted in Fig. 2 the dislocations concentrate around the crack's process zone and form a complex interconnected cell structure, well documented to occur in f.c.c. materials for large static and cyclic plastic deformation. Also, high concentrations of plastic deformation on both sides of the grain boundary and the crack flanks can be observed, unexpectedly similar to macroscopic crack behavior. The tomography proved activity on multiple slip systems. Therefore, further deconvolution of slip system coupling is not possible for a stage-II fatigue crack.

4. Conclusion

From the crack growth curves of these *in situ* micro bending fatigue tests, coupled with HR-EBSD-tomography we can conclude:
- da/dN curves can be measured in micro specimens by a combination of elaborated *in situ* testing, compliance method and FEM.

- The misorientation alone is no suitable measure for slip transfer across grain boundaries, the resulting deceleration of crack growth rate (Schaefer et al. (2017)), and thus for the crack growth resistance for stage-II fatigue cracks.
- A very complex dislocation structure causes the slope of the crack growth curve to increase relative to the macroscopic case of m=2 for f.c.c. materials (Marx and Vehoff (2003)), depending on the crystallographic orientation and the number of equivalent slip systems.

We are now able to use the presented method for examination of highly localized phenomena such as hydrogen induced embrittlement of grain boundaries or influence of high stress and strain concentration from a crack on microstructural stability e.g. in nanocrystalline materials.

Acknowledgments

References

Schaefer, F., Lang, E. P., Bick, M., Knorr, A. F., Marx, M., Motz, C., 2017. Assessing the intergranular crack initiation probability of a grain boundary distribution by an experimental misalignment study of adjacent slip systems. Procedia Structural Integrity 5, 547-554.

Knorr, A. F., Marx, M., Schaefer, F., 2015. Crack initiation at twin boundaries due to slip system mismatch. Scripta Materialia 94, 48-51.

Zhang, Z. F., Wang, Z. G., Hu, Y. M., 1999. Fatigue crack initiation and fracture behavior of a copper bicrystal with a perpendicular grain boundary. Materials Science and Engineering: A 269(1-2), 136-141.

Kacher, J., Robertson, I. M., 2012. Quasi-four-dimensional analysis of dislocation interactions with grain boundaries in 304 stainless steel. Acta Materialia 60(19), 6657-6672.

Schaef, W., Marx, M., Vehoff, H., Heckl, A., Randelzhofer, P., 2011. A 3-D view on the mechanisms of short fatigue cracks interacting with grain boundaries. Acta Materialia 59(5), 1849-1861.

Klusemann, B., Svendsen, B., Vehoff, H. 2013. Modeling and simulation of deformation behavior, orientation gradient development and heterogeneous hardening in thin sheets with coarse texture. International Journal of Plasticity 50, 109-126.

Tiba, I., Richeton, T., Motz, C., Vehoff, H., Berbenni, S., 2015. Incompatibility stresses at grain boundaries in Ni bicrystalline micropillars analyzed by an anisotropic model and slip activity. Acta Materialia 83, 227-238.

Brueck, S., Schippl, V., Schwarz, M., Christ, H. J., Fritzen, C. P., Weihe, S.,2018. Hydrogen Embrittlement Mechanism in Fatigue Behavior of Austenitic and Martensitic Stainless Steels. Metals 8(5), 339.

Krupp, U., Knobbe, H., Christ, H. J., Koester, P., Fritzen, C. P., 2010. The significance of microstructural barriers during fatigue of a duplex steel in the high-and very-high-cycle-fatigue (HCF/VHCF) regime. International Journal of Fatigue 32(6), 914-920.

Zerbst, U., Vormwald, M., Pippan, R., Gaenser, H. P., Sarrazin-Baudoux, C., Madia, M., 2016. About the fatigue crack propagation threshold of metals as a design criterion–a review. Engineering Fracture Mechanics 153, 190-243.

Schaefer, F., Thielen, M., Marx, M., Motz, C., 2017. How to Measure a Dislocation's Breakthrough Stress to Estimate the Grain Boundary Resistance against Slip Transfer Based on the DFZ-Model of Fracture. Solid State Phenomena 258, 93-96.

Holzapfel, C., Schaef, W., Marx, M., Vehoff, H., Muecklich, F., 2007. Interaction of cracks with precipitates and grain boundaries: Understanding crack growth mechanisms through focused ion beam tomography. Scripta Materialia 56(8), 697-700.

Schaefer, F., Weiter, L., Marx, M., Motz, C., 2016. Quantifying the grain boundary resistance against slip transfer by experimental combination of geometric and stress approach using stage-I-fatigue cracks. Philosophical Magazine 96(32-34), 3524-3551.

Schaef, W., Marx, M., Vehoff, H., Heckl, A., Randelzhofer, P., 2011. A 3-D view on the mechanisms of short fatigue cracks interacting with grain boundaries. Acta Materialia 59(5), 1849-1861.

Eisenhut, L., Schaefer, F., Gruenewald, P., Weiter, L., Marx, M., Motz, C., 2017. Effect of a dislocation pile-up at the neutral axis on trans-crystalline crack growth for micro-bending fatigue. International Journal of Fatigue 94, 131-139.

Gruenewald, P., Schaefer, F., Thielen, M., Marx, M., Motz, C., 2018. Small scale fracture mechanics of ductile materials: Advantage of fatigue precracks and comparison of J-integral evaluations. Materialia 4, 104-108.

Pantleon, W., 2008. Resolving the geometrically necessary dislocation content by conventional electron backscattering diffraction. Scripta Materialia 58(11), 994-997.

Wilkinson, A. J., Meaden, G., Dingley, D. J., 2006. High-resolution elastic strain measurement from electron backscatter diffraction patterns: New levels of sensitivity. Ultramicroscopy 106(4-5), 307-313.

Wilkinson, A. J., Dingley, D. J., Meaden, G., 2009. Strain mapping using electron backscatter diffraction. Electron Backscatter Diffraction in Materials Science, 231-249.

Marx, M., Vehoff, H., 2004. Propagation of microcracks in single crystalline nickel-based superalloys: size effects on the crack opening. Materials Science and Engineering: A 387, 511-515.